Neuropsychologia 89 (2016) 495–509

Contents lists available at ScienceDirect

Neuropsychologia

journal homepage: www.elsevier.com/locate/neuropsychologia

Early differential sensitivity of evoked-potentials to local and global shape during the perception of three-dimensional objects

E. Charles Leek [a,c,*], Mark Roberts [a], Zoe J. Oliver [a], Filipe Cristino [a], Alan J. Pegna [b]

[a] Wolfson Centre for Clinical and Cognitive Neuroscience, School of Psychology, Bangor University, UK
[b] Department of Psychology, University of Queensland, Brisbane, Australia
[c] Laboratoire de Psychologie et NeuroCognition (LPNC), Université Grenoble Alpes, France

ARTICLE INFO

Article history:
Received 8 February 2016
Received in revised form
29 June 2016
Accepted 6 July 2016
Available online 7 July 2016

Keywords:
3D shape perception
Global configuration
Local part structure
Evoked potentials

ABSTRACT

Here we investigated the time course underlying differential processing of local and global shape information during the perception of complex three-dimensional (3D) objects. Observers made shape matching judgments about pairs of sequentially presented multipart novel objects. Event-related potentials (ERPs) were used to measure perceptual sensitivity to 3D shape differences in terms of local part structure and global shape configuration – based on predictions derived from hierarchical structural description models of object recognition. There were three types of different object trials in which stimulus pairs (1) shared local parts but differed in global shape configuration; (2) contained different local parts but shared global configuration or (3) shared neither local parts nor global configuration. Analyses of the ERP data showed differential amplitude modulation as a function of shape similarity as early as the N1 component between 146–215 ms post-stimulus onset. These negative amplitude deflections were more similar between objects sharing global shape configuration than local part structure. Differentiation among all stimulus types was reflected in N2 amplitude modulations between 276–330 ms. sLORETA inverse solutions showed stronger involvement of left occipitotemporal areas during the N1 for object discrimination weighted towards local part structure. The results suggest that the perception of 3D object shape involves parallel processing of information at local and global scales. This processing is characterised by relatively slow derivation of 'fine-grained' local shape structure, and fast derivation of 'coarse-grained' global shape configuration. We propose that the rapid early derivation of global shape attributes underlies the observed patterns of N1 amplitude modulations.

1. Introduction

The human visual system is remarkably good at distinguishing among visually similar three-dimensional (3D) objects across changes in the sensory input (e.g., Arguin and Leek, 2003; Bar, 2003; Bar et al., 2006; Cichy et al., 2014; Cristino et al., 2015; Fabre-Thorpe, 2011; Harris et al., 2008; Kirchner and Thorpe, 2006; Leek, 1998a, 1998b; Leek et al., 2015, 2007; Leek and Johnston, 2006; Tarr and Bulthoff, 1998; Thorpe et al., 1996; VanRullen and Thorpe, 2001). This ability relies fundamentally on sophisticated perceptual processes that compute mental representations of 3D object shape.

In principle, 3D objects comprise different kinds of shape information (e.g., Arguin and Saumier, 2004; Biederman, 1987; Davitt et al., 2014; Edelman, 1999; Hummel, 2013; Hummel and Stankiewicz, 1996; Leek et al., 2012a, 2012b, 2009, 2005; Lloyd-Jones and Luckhurst, 2002; Marr and Nishihara, 1978; Pizlo, 2008; Reppa et al., 2014; Schendan and Kutas, 2007; Ullman, 2006). This information varies in the spatial scale at which it is likely to be computed. For example, we can distinguish between 'local' information sampled from relatively small regions of the sensory input, and 'global' information sampled from larger regions - along a continuous spatial scale (e.g., from a single image point to an entire object). Sampling at relatively small scales might include information about edge boundaries, vertices, surface curvature, slant, part boundaries and local part shape. In contrast, sampling at larger scales might include information about global object properties such as the overall spatial configuration, axes of elongation and symmetry, orientation, aspect ratio and size.

Currently, we know relatively little about how shape information across these different scales, or levels of representation, is computed and integrated during the perception of complex 3D object shape. Some potentially relevant evidence comes from research with other classes of stimuli. For example, prior studies of scene perception have shown that observers can rapidly classify

* Corresponding author at: Wolfson Centre for Clinical and Cognitive Neuropsychology, School of Psychology, Bangor University, Bangor LL572AS, UK.
E-mail address: e.c.leek@bangor.ac.uk (E.C. Leek).

http://dx.doi.org/10.1016/j.neuropsychologia.2016.07.006

scenes based on coarse analyses of global (i.e., low spatial frequency) image content (e.g., Bullier, 2001; Hegde, 2008; Heinz et al., 1994, 1998; Lamb and Yund, 1993; Peyrin et al., 2010, 2004, 2003; Schyns and Oliva, 1994). Similarly, studies using hierarchical displays in which, for example, observers report either local or global information from congruent or incongruent arrays (e.g., a larger letter H comprised of either small Hs or Ts - Navon, 1977) have provided evidence for the precedence of global information processing during visual perception. Other work has shown early perceptual sensitivity to local and global stimulus structure in hierarchical displays within 200 ms of display onset (e.g., Beaucousin et al., 2013; Han et al., 2000; Proverbio et al., 1998; Yamaguchi et al., 2000), asymmetric involvement of the left and right hemispheres in the processing of local and global display properties (e.g., Fink et al., 1996; 1997; Kimchi and Merhav, 1991; Han et al., 2002; Heinz et al., 1994; 1998), and dissociations between the reporting of local and global elements of complex displays in patients with unilateral lesions (Robertson et al., 1988; Robertson and Lamb, 1991).

However, the direct relevance of these studies to our understanding of differential processing of local and global properties of complex 3D object shapes is unclear. For example, scene classification is likely to be constrained by contextual information that is not available to processes involved in computing 3D object shape, and in previous studies using hierarchical displays, unlike in everyday object recognition, observers are explicitly instructed to attend to, and report, incongruent local or global display elements.

Our aim was to investigate the processing of local and global shape information during the perception of complex 3D objects. In particular, we tested the hypothesis that the perceptual analysis of 3D object shape should show evidence of differential processing of local part structure and global shape configuration. To examine this we used a discrimination task in which observers made shape matching judgements about pairs of sequentially presented surface rendered, multi-part, novel objects. We recorded ERPs to provide an online measure of perceptual processing. On each trial, the stimuli could be the same or different objects. On different object trials, shape similarity was manipulated in terms of same or different local part structure and/or global shape configuration. The rationale was based on comparing evoked potentials for repetitions of the same object relative to those for different object pairs as a function of object shape similarity. ERP responses to different object pairs that share local part structure, but not global shape configuration, provide a measure of perceptual sensitivity to local shape properties. In contrast, responses to different object pairs that share global shape configuration, but not local part structure, provide a measure of perceptual sensitivity to global shape properties. Using this approach we were able to obtain implicit measures of perceptual sensitivity to local and global shape information that avoided explicitly directing perceptual processing towards either level of representation.

2. Methods

2.1. Subjects

Twenty participants (10 male; 19 right handed, Mean age=26; SD=7) took part in the experiment for course credit. None had a previous history of neurological or psychiatric disorder. All had normal or corrected-to-normal visual acuity. The study was approved by the Ethics Committee of the School of Psychology, Bangor University. The protocol was fully compliant with the ethics guidelines of the British Psychological Society and the Declaration of Helsinki (1964). Participants provided written informed consent, and were free to withdraw from the study at any time.

2.2. Apparatus

EEG signals were acquired using a 64-channel NeuroScan SynAmps2 system (Neuroscan Inc.) – see below for acquisition and online/offline filtering parameters. The EEG data were recorded in a fully shielded and sound attenuated room. Two Dell Precision 380 workstations controlled stimulus presentation and data acquisition. Stimuli were displayed on a Hitachi 17 CRT monitor running at 1280×1024 (32 bit colour depth) resolution. A standard QWERTY PC keyboard was used to acquire behavioural responses. The experiment was programmed and run using E-prime (v.1.1; www.pstnet.com/eprime).

2.3. Stimuli

The stimuli comprised a total set of 48 CAD generated 3D surface rendered, four part, novel objects. This comprised 12 sets each composed of four different objects (see Fig. 1). Each object comprised four volumetric parts defined by variation among non-accidental properties (NAPs): Edges (straight vs. curved), symmetry of the cross section, tapering (co-linearity) and aspect ratio (Biederman, 1987). The use of novel object stimuli, rather than images of familiar common objects, allowed us to carefully control the geometric properties of the stimulus set, and reduce potential influences of pre-established visual-semantic associations.

The models were designed in Strata 3D CX software (Strata Inc. USA) and rendered with shading over smooth surfaces in a mustard yellow colour (RGB: 227, 190, 43). This was done to prevent obscuring object internal structure (e.g., part boundaries at local surface discontinuities). The lighting model used a single light source in the top left quadrant. Stimuli were scaled to have the same maximum dimensions of 7.5° by 7.5° from a viewing distance of 60 cm. Stimuli were displayed on a white background to enhance figure/ground contrast, and to ensure that object bounding contour could be clearly identified.

Each of the 12 object sets were comprised of one base ('target') object and three other ('distracter') stimuli. The distracters were created by factorial variation of similarity to their respective target in terms of local volumetric parts and/or global shape configuration. We refer to the base objects as 'SS' stimuli. The distracter conditions were: 'SD' (Same local/Different global – locally similar) which shared parts but had a different global shape configuration to the corresponding base object; 'DS' (Different local/Same global – globally similar) which shared global shape configuration but had different parts; 'DD' (Different local/Different global) which shared neither parts nor global shape configuration with the corresponding base. Fig. 2 illustrates the different trial types.

These stimulus contrasts allowed us to examine perceptual sensitivity to different types of similarity relations in terms of shared local part structure and/or global shape configuration. Each stimulus was rendered at a viewpoint chosen to ensure visibility of the local parts and global spatial configuration, and to minimise self-occlusion (see Fig. 1). We also created four masks each composed of random configurations of NAP-defined part elements from the object set. The purpose of the masks was to delineate the onset of the second stimulus in the trial sequence, and to reduce the likelihood that participants would be able to make shape matching judgements based on a direct pixel-to-pixel matching strategy. For the same reason, stimuli were displayed at different scales: S1=600×600 pixels; S2=400×400 pixels.

2.4. Design and procedure

The design involved manipulating the relationship between

Fig. 1. The 48 item novel object set used in the study.

Fig. 2. Illustration of the stimulus types: Stimulus conditions (SD, DS and DD) are denoted by local and global shape similarity to the base (SS) objects. The locally similar objects (SD) share local parts but not global configuration. The globally similar objects (DS) share global configuration but not local parts. The DD stimuli share neither local parts nor global spatial configuration.

two sequentially presented objects (S1, S2). During the experimental trials S1 always comprised an SS stimulus (see Fig. 1). S2 stimuli could be either SS ('Same' response) or one of three 'Different' response stimuli: SD (locally similar), DS (globally similar) and DD. In total there were 288 trials divided equally into two blocks of 144 trials each. Across blocks there were 48 trials per

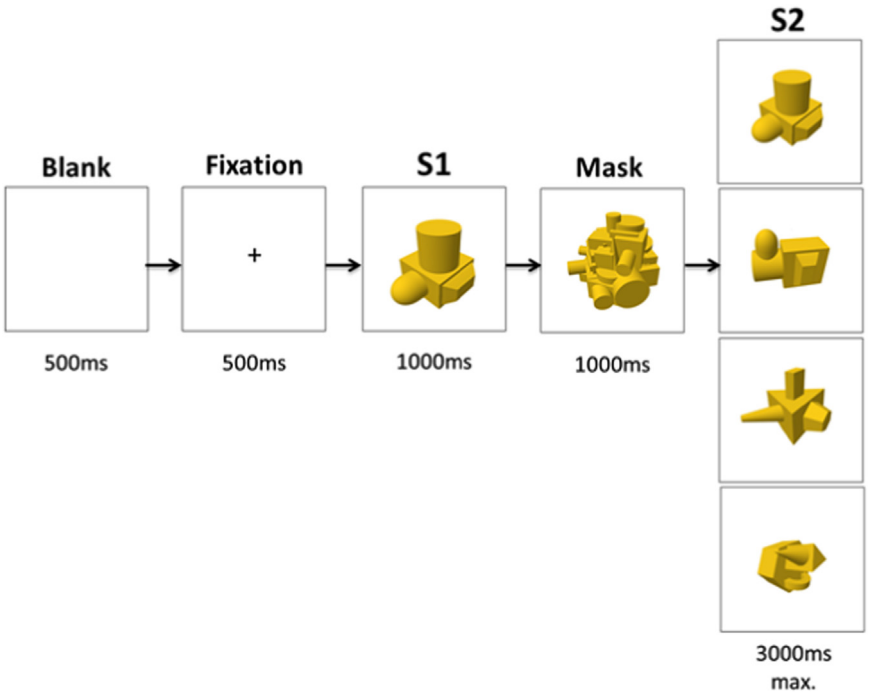

Fig. 3. The trial structure (see text).

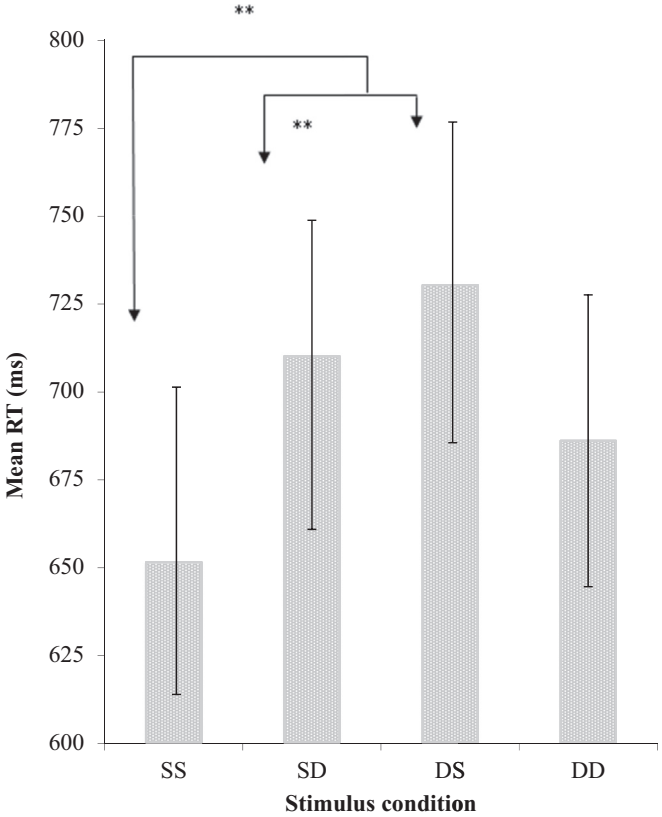

Fig. 4. Mean RTs for correct responses as a function of stimulus condition (SS – Same local/Same global – base; SD – Same local/Different global – locally similar; DS – Different local/Same global – globally similar; DD – Different local/Different global). Bars show standard error of the mean.

condition. In order to avoid a response bias or associated 'expectancy' effects in the ERPs we equated the number of 'Same' and 'Different' trials by including 96 'Same' response filler trials in each block. These used 3D object models constructed and rendered identically to the experimental stimulus set. These items were not included in the analyses. In total (including fillers) there were 144 'Same' and 144 'Different' response trials across blocks, with equal numbers of trials per condition for the analysis. Fig. 3 shows the basic trial structure.

A chin rest was used to maintain a viewing distance of 60 cm. Before the main task, observers completed 12 practice trials using three additional novel objects and masks that were not included in the main experiment. Each trial started with a centrally presented black fixation cross (Courier New, 18 point font; 500 ms) followed by S1 (1s), a mask (1s) and then S2. S2 remained on the screen until the participant responded by pressing one of two keys (f or j) on a standard PC keyboard labelled 'Same' and 'Different'(max 3s). A blank ISI of 100 ms separated each visible screen display event (Fixation, S1, Mask, and S2). There was a blank inter-trial interval of 1 s. At the end of each trial feedback was provided in the centre of the monitor for 500 ms. This indicated incorrect responses only accompanied by a short beep. Half of the participants responded 'Same' with their left index finger and 'Different' with their right index finger. This order was reversed for the other half. Trial order was randomised. The total duration of the testing session was approximately 90 min.

2.5. EEG-ERP acquisition

EEG signals were sampled at 1024 Hz from 64 Ag/AgCl electrodes referenced to Cz and placed according to the extended 10–20 convention (American Electroencephalographic Society, 1991: TP7, FT7, AF7, FCz, AF8, FT8, TP8, C5, F5, AF3, CPz, AF4, F6, C6, CP3, C1, FC3, POz, FC4, C2, CP4, TP9, PO7, P5, Oz, P6, PO8, TP10, P1, PO3, PO4, P2, FT9, F7, Fp1, AFz, Fp2, F8, FT10, T7, FC5, F3, Fz, F4, FC6, T8, CP5, C3, FC1, Pz, FC2, C4, CP6, P7, P3, CP1, O1, CP2, P4, P8, Iz, PO9, O2, PO10). Impedances were below 9 kΩ. Signals were filtered online between 0.01 and 100 Hz, data was filtered off line using a 30 Hz low pass filter with a slope of 12 db/oct. Ocular artifacts were mathematically corrected using Scan 4.3 software (Neuroscan, Inc.) based on an algorithm developed by Gratton et al. (1983). Remaining artifacts were manually rejected upon visual

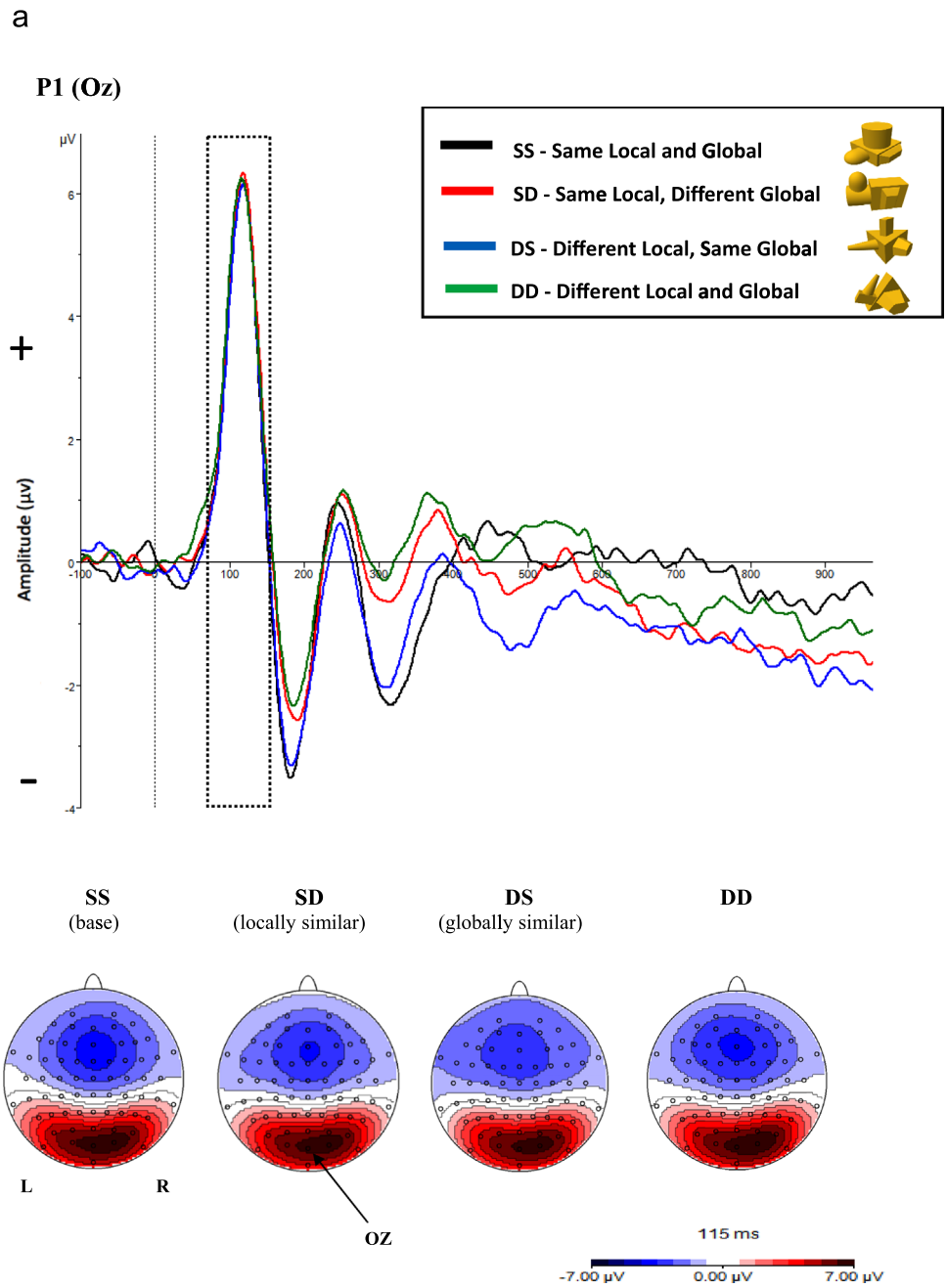

Fig. 5. (a) Grand average ERPs (top) and associated topographies (bottom) as a function of stimulus type for the (a) P1 (70–145 ms; recorded at electrode Oz; topography at 115 ms), (b) N1 (146–215 ms; PO8; topography at 180 ms), (c) P2 (216–275 ms, PO4; topography at 250 ms), and (d) N2 (276–330 ms, P8; topography at 310 ms). Arrows indicate the position of the electrode shown for each component.

inspection. EEG epochs ranging from −100 (prior to S2 onset) to 1000 ms relative to stimulus onset were baseline corrected in reference to pre-stimulus activity before ERP averaging. Finally, ERPs were re-referenced to the global average reference. Peak detection was carried out automatically, time-locked to the latency of the peak at the electrode of maximal amplitude on the grand average ERP (Picton et al., 2000). Triggers were recorded during EEG data acquisition marking the onset of S1 and S2, stimulus condition and response accuracy.

2.6. ERP analysis

The four main early visual ERP components P1, N1, P2 and N2, were identified based on the topography, deflection and latency characteristics of the respective grand average ERPs time-locked to stimulus presentation. Epochs of interest for each component were defined on the basis of deflection extrema in the mean global field power (MGFP) (Picton et al., 2000). Peak detection was time-locked to the electrode of maximal amplitude for each component; P1: 70–145 ms maximal at electrode Oz (mean peak 115 ms); N1: 146–215 ms maximal at electrode PO8 (mean peak 180 ms); P2: 216–275 ms maximal at electrode P3 (mean peak 245 ms); and N2: 276–330 ms maximal at electrode PO8 (mean peak 305 ms). Peak mean amplitudes and latencies were analysed using Stimulus Type (SS, DS, SD, DD) × ELECTRODE LATERALITY (right, left) as factors in repeated measures ANOVA. Electrodes used for each component were: P1: O1, Oz, O2; N1: PO7, O1, P7, PO8, O2, P8; P2: P1, P3, PO3, P2, P4, PO8; and N2: P3, P5, PO3, PO7, P4, P6, PO4, PO6. Channel selection was based on initial inspection of the topographies with electrode clusters centred on the site showing the peak

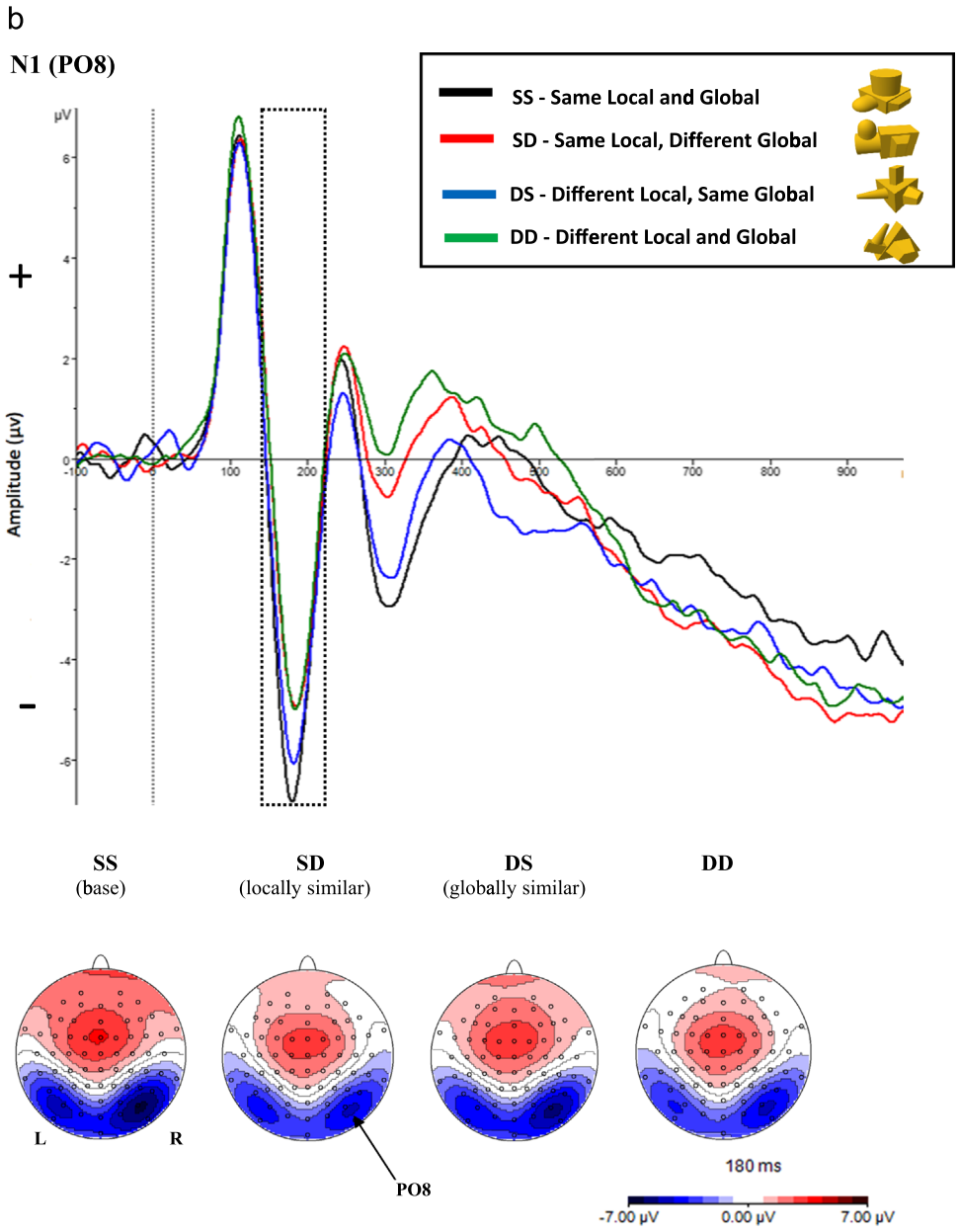

Fig. 5. (*continued*)

amplitudes within the selected time window for each component with a corresponding cluster in the opposite hemisphere. Greenhouse-Geisser corrections were applied to all ERP data analyses. Unless otherwise stated only significant main effects and interactions are reported where corrected $\alpha < 0.05$. Exact values of p are reported, except where $p < 0.001$ (two tailed).

2.7. Source localisation

To explore the underlying neural generators for the scalp topographies we used the Standardised Low Resolution Brain Electromagnetic Tomography linear inverse solution (sLORETA; Pascual-Marqui, 2002). sLORETA provides a single linear solution that has been shown to estimate the underlying source of surface EEG topographies with high localisation accuracy (e.g., Sekihara et al., 2005; Vitacco et al., 2002; Wagner et al., 2004). Intra-cerebral cerebral volume is partitioned into 6239 voxels of 5 mm^3 spatial resolution, and standardized current density per voxel is computed within a realistic head model (Fuchs et al., 2002) using the Montreal Neurological Institute MNI152 template (Jurcak et al., 2007; Mazziotta et al., 2001).

3. Results

3.1. RTs and accuracy

Overall accuracy was high ($M = 96.69\%$, $SD = 1.25$). There were no significant differences in mean accuracy across conditions. Analyses of RTs involved data from correct responses only.[1]

Fig. 4 shows mean RTs per condition.

A one-way ANOVA across conditions (SS, DS, SD, DD) was significant, $F(4, 16) = 62.11$, $p < 0.001$, $\eta p^2 = 0.93$. Mean RTs for SS base objects ($M = 651.28$ ms, $SD = 183.31$) were significantly faster than

[1] The patterns of behavioural and ERP data for the left-handed participant and the group were the same across conditions.

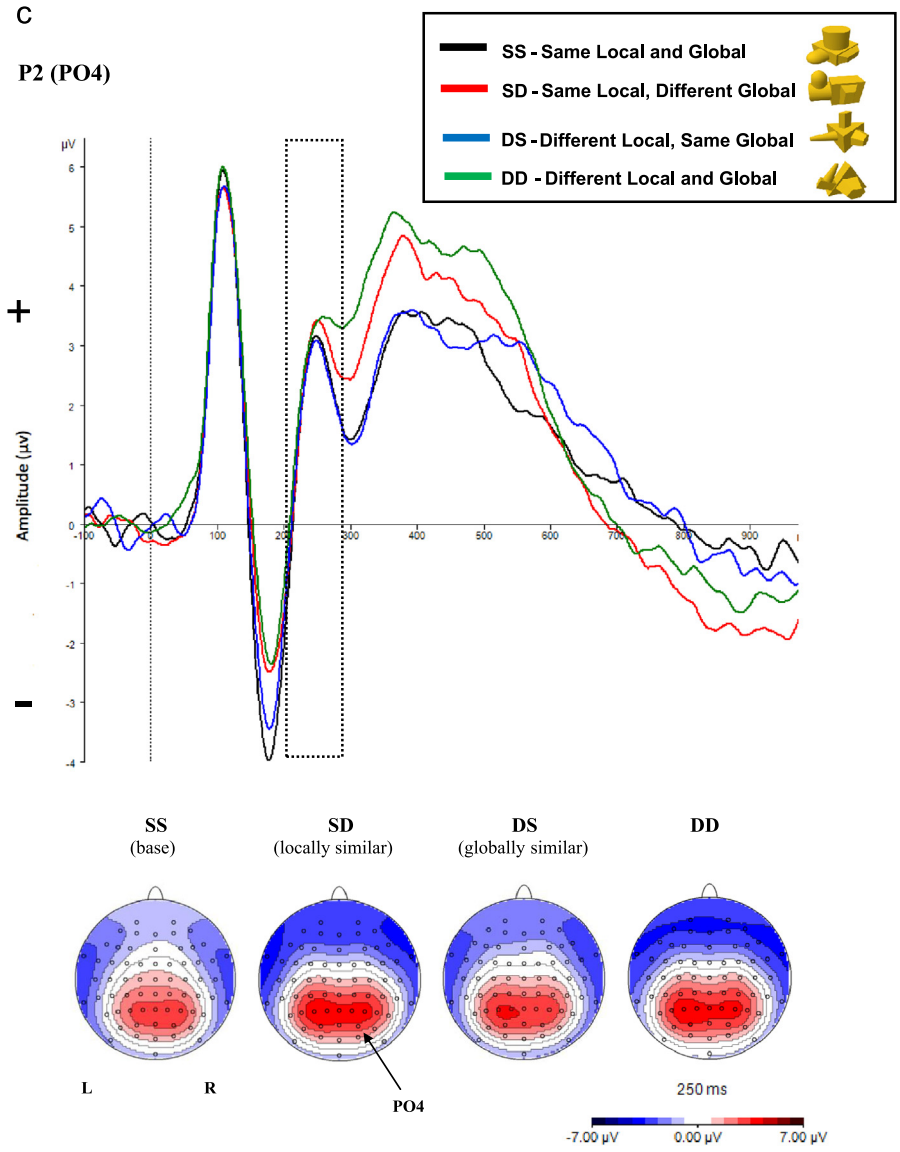

Fig. 5. (*continued*)

the SD (locally similar: $M=709.85$ ms, $SD=191.54$), t (19)=3.19, $p=.004$; and DS (globally similar: $M=730.07$ ms, $SD=198.75$), t (19)=5.97, $p<0.001$; different object conditions, but not DDs ($M=685.80$ ms, $SD=180.86$), t (19)=1.7, *ns.*). There was also a significant difference between SD (locally similar) and DS (globally similar) stimuli, (t (19)=2.36, $p=02$) indicating faster responses to SD (locally similar) over DS (globally similar) objects.

3.2. Event-related potentials

3.2.1. Standard waveform analyses

Peak detection was time-locked to the electrode of maximal amplitude for each component within the epochs of interests (see above). Fig. 5a–d shows the grand average ERP traces and associated topographies for each of the four components of interest (P1, N1, P2, N2).

3.2.1.1. P1 (70–145 ms)

3.2.1.1.1. Latencies. Mean peak latencies were: SS=114.5 ms ($SD=8.2$), SD=(locally similar) 117 ms (SD=7.39), DS (globally similar)=115.7 ms ($SD=8.2$) and DD=115.9 ms ($SD=7.27$). There were no significant differences between conditions.

3.2.1.1.2. Amplitudes. There were no significant differences.

3.2.1.2. N1 (146–215 ms)

3.2.1.2.1. Latencies. Mean peak latencies were: SS=181 ms ($SD=11.5$), SD (locally similar)=183.4 ms ($SD=11.86$), DS (globally similar)=180.3 ms ($SD=11.69$) and DD=183.65 ms ($SD=9.56$). There were no significant differences.

3.2.1.2.2. Amplitudes. There were significant main effects of Stimulus type (SS, SD, DS, DD), F (3, 19)=15.66, $p<0.001$, $\eta p^2=0.45$, and Laterality, F (1, 19)=4.821, $p=.041$, $\eta p^2=0.20$, but no significant interactions. Further planned comparisons showed significant differences between: SS-SD (locally similar): F (1, 19)=24.64, $p<0.001$, $\eta p^2=0.565$; SS-DS (globally similar): F (1, 19)=5.24, $p=.034$, $\eta p^2=0.216$; SS-DD: F (1, 19)=29.28, $p<0.001$, $\eta p^2=0.60$; SD-DS: F (1, 19)=9.988, $p=.005$, $\eta p^2=0.345$; DS-DD: F (1, 19)=17.844, $p<0.001$, $\eta p^2=0.60$, but not SD-DD.

3.2.1.3. P2 (216–275 ms)

3.2.1.3.1. Latencies. Mean peak latencies were: SS=244.5 ms ($SD=17.63$), SD (locally similar)=252.95 ms ($SD=19.65$), DS (globally similar)=248.6 ms ($SD=15.51$) and DD=253.6 ms ($SD=19.67$). There were no significant differences.

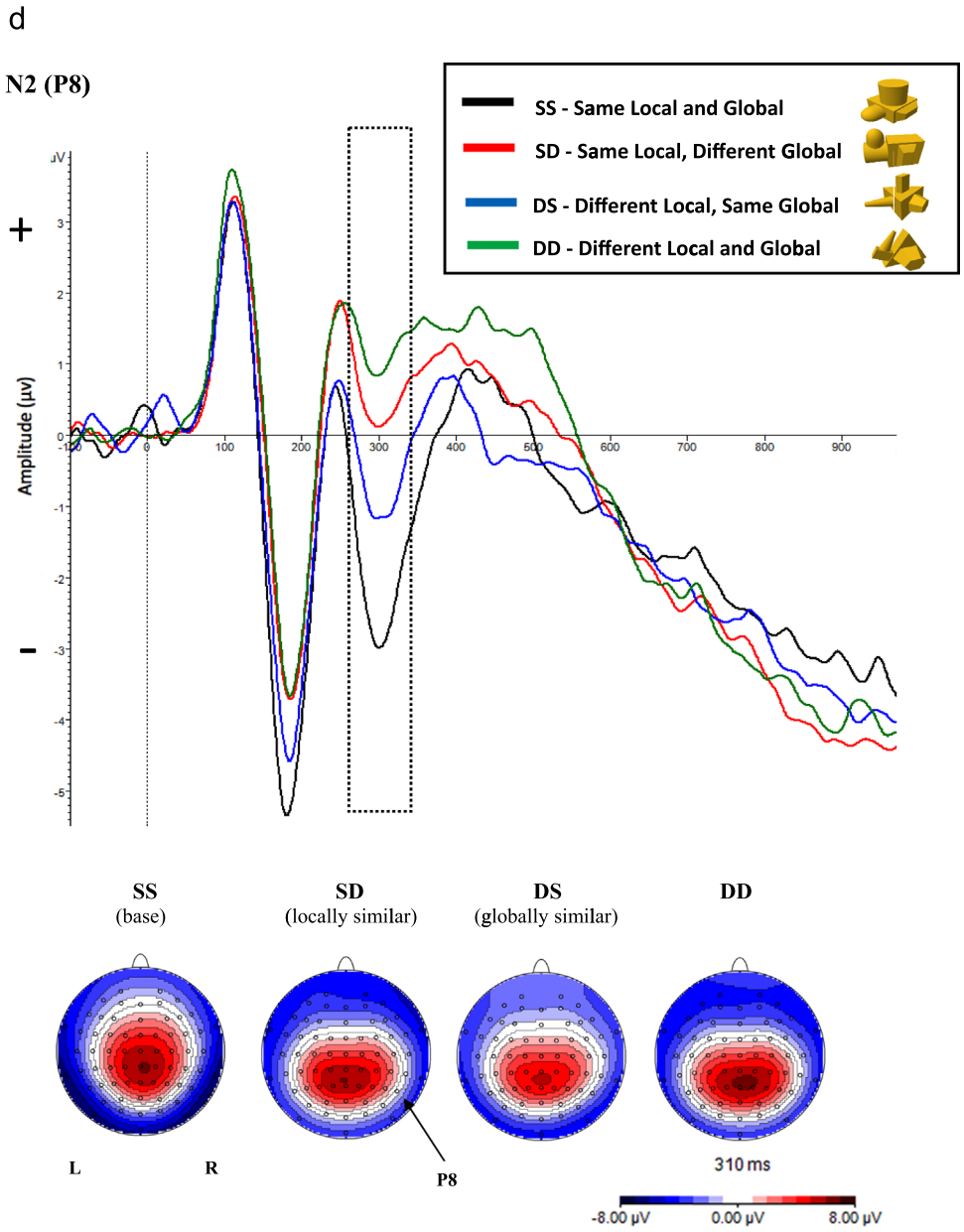

Fig. 5. (*continued*)

3.2.1.3.2. Amplitudes. There was a significant main effect of Stimulus type, F (3, 19)=6.19, p=.002, ηp^2=0.24, but no main effect of laterality and no interaction. Further planned contrasts showed significant differences between: SS-SD (locally similar): F (1, 19)=7.47, p=.013, ηp^2=0.28; SS-DD: F (1, 19)=8.94, p=.008, ηp^2=0.32; SD-DS: F (1, 19)=6.35, p=.021, ηp^2=0.25; DS-DD: F (1, 19)=11.64, p=.003, ηp^2=0.38. The contrasts between SS-DS (globally similar) and SD-DD were not significant.

3.2.1.4. N2 (276–330 ms)

3.2.1.4.1. Latencies. Mean peak latencies were: SS=300.15 ms (*SD*=13.30), SD (locally similar)=298.75 ms (*SD*=16.62), DS (globally similar)=305.2 ms (*SD*=11.83) and DD=299.15 ms (*SD*=15.11). There were no significant differences.

3.2.1.4.2. Amplitudes. There was a significant main effect of Stimulus type, F (3, 19)=20.09, p < 0.001, ηp^2=0.51, but no main effect of laterality and no interaction. Further planned contrasts showed significant differences between all pairs of conditions: SS-SD (locally similar): F (1, 19)=23.40, p < 0.001, ηp^2=0.55; SS-DS (globally similar): F (1, 19)=7.29, p=.014, ηp^2=0.27; SS-DD: F (1, 19)=28.03, p < 0.001, ηp^2=0.59; SD-DS: F (1, 19)=16.00, p < 0.001, ηp^2=0.45; SD-DD: F (1, 19)=4.81, p=.04, ηp^2=0.20; DS-DD: F (1, 19)=23.717, p < 0.001, ηp^2=0.72.

There was no statistical evidence of any pre-motor effects whether in the form of a slow negativity or a sharp ipsilateral positivity corresponding to the hand of response.

3.2.2. Source localisation analysis

In light of the significant laterality effect on N1 amplitudes, we wanted to explore potential differences in the focal neural generators of the processes underlying processing of SD (locally similar) and DS (globally similar) objects during the N1 time window. Fig. 6 shows the sLORETA inverse solutions for the N1 component using 5 mm slices on the MNI2009 T1 scan from Z=−20 to Z=0. The SD and DS conditions are highlighted in the dashed red box for ease of comparison. This shows a pattern of asymmetrical bilateral activity across conditions. In particular, the DS (globally similar) condition elicited greater activity relative to the

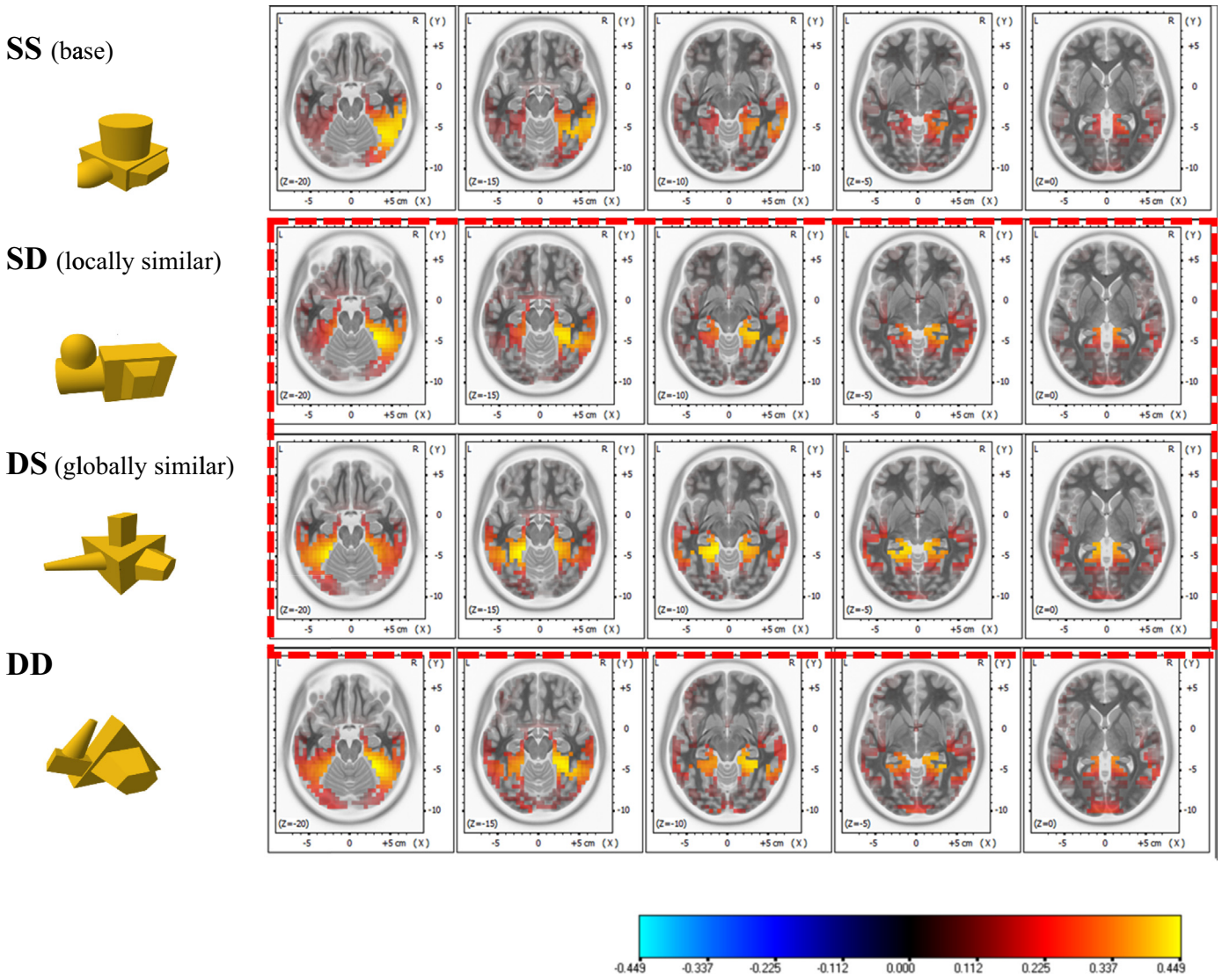

Fig. 6. sLORETA inverse solutions for the *N1* (180 ms post-stimulus onset) component plotted using the MNI1152–2009 T1 template for each stimulus condition. Axial slices (5 mm) shown at Z = −20 to Z = 0. Colour coding shows standardized current density. (For interpretation of the references to color in this figure legend, the reader is referred to the web version of this article.)

SD (locally similar) condition in the left posterior temporal-occipital cortex encompassing the medial lingual gyrus and posterior fusiform gyrus. To explore this further sLORETA was used to compute voxel-wise contrasts between the SD (locally similar) and DS (globally similar) conditions during the N1 time window. This was based on 5000 permutations using statistical non-parametric mapping tests for paired samples with correction for multiple comparisons (Holmes et al., 1996). Voxels with significant differences ($p < 0.05$, corrected; t-threshold = 6.58) between SD (locally similar) and DS (globally similar) were located in MNI coordinates. Table 1 lists locations of the voxels exceeding criterion threshold for significance. For each region the MNI coordinates, Brodmann area and associated t-values are given.

Fig. 7 shows the t-map distribution using the sLORETA head model. This indicates that processing of the DS (globally similar) relative to SD (locally similar) stimuli is more strongly associated with left hemisphere posterior temporal-occipital sites. Finally, we also computed the inverse solutions associated with the N2 component during the 276–330 ms time window. During this time window the ERP amplitudes for each condition were reliably distinguishable from each other, indicating a possible temporal marker for image classification.

Fig. 8 shows the sLORETA inverse solutions for the N2 component plotted using the MNI1152-2009 T1 template for each stimulus condition. This shows very similar bilateral patterns of activity across conditions that are more strongly localised to the right inferotemporal cortex. Unlike the N1, voxel-wise contrasts between the SD (locally similar) and DS (globally similar) conditions during the N2 showed no statistically significant differences.

To further explore the N2 inverse solutions we also used sLORETA to compute pairwise voxel-by-voxel contrasts between the SS/SD (locally similar), SS/DS (globally similar) and SS/DD conditions.

The t maps (showing locations of maximal values) for these contrasts are shown in Fig. 9. The SS/DS (globally similar) contrast showed significant ($p < 0.05$) corrected differences in activity (SS > DS) along the occipito-temporal ventral pathway of the right hemisphere encompassing the inferior and middle temporal gyri, fusiform gyrus and parts of the parahippocampal gyrus. Neither the SS/SD (locally similar) nor SS/DD contrasts showed maximum t values exceeding the corrected significance threshold (ps > 0.1). An additional analysis contrasting the SD (locally similar) and DS (globally similar) conditions also failed to show any significant differences.

Table 1
Summary of regions showing significantly greater activity in the DS relative to the SD condition during the N1 time window (146–215 ms). All statistics are derived from the sLORETA inverse solutions ($p < 0.05$, corrected, t-threshold = 6.58). The table shows the anatomical label, Brodmann area (BA), MNI coordinates and associated t-value of the voxels within each region showing maximal values.

Region		BA	X	Y	Z	t-value
Left hemisphere						
Occipital lobe	Fusiform gyrus	18	−20	−95	−20	−7.12
Occipital lobe	Fusiform gyrus	18	−25	−95	−20	−6.83
Temporal lobe	Fusiform gyrus	37	−55	−55	−25	−6.77
Temporal lobe	Fusiform gyrus	37	−50	−60	−25	−6.62
Temporal lobe	Fusiform gyrus	37	−55	−50	−25	−6.60
Temporal lobe	Fusiform gyrus	37	−50	−55	−25	−6.60
Occipital lobe	Lingual gyrus	18	−10	−100	−15	−7.77
Occipital lobe	Lingual gyrus	18	−5	−95	−20	−7.51
Occipital lobe	Lingual gyrus	17	−10	−95	−20	−7.38
Occipital lobe	Lingual gyrus	17	−15	−95	−20	−7.32
Occipital lobe	Lingual gyrus	17	−10	−95	−15	−7.03
Occipital lobe	Lingual gyrus	18	10	−100	−10	−6.97
Occipital lobe	Lingual gyrus	18	−10	−100	−10	−6.88
Occipital lobe	Lingual gyrus	17	−15	−95	−15	−6.86
Right hemisphere						
Occipital lobe	Fusiform gyrus	18	20	−95	−20	−6.68
Occipital lobe	Lingual gyrus	18	5	−95	−15	−7.07
Occipital lobe	Lingual gyrus	17	10	−95	−15	−6.80
Occipital lobe	Lingual gyrus	18	15	−100	−10	−6.75
Occipital lobe	Lingual gyrus	17	15	−95	−15	−6.69

4. Discussion

The main findings can be summarised as follows: First, the ERP data showed differential sensitivity to local part structure and global shape configuration as early as the N1 component on posterior electrodes 146–215 ms post-stimulus onset. Second, the patterns of amplitude modulation during the N1 showed greater similarity between SS (base) and DS (globally similar) objects, than between SS (base) and either SD (locally similar) or DD objects that shared neither local parts nor global shape configuration. Third, the behavioural data showed longer RTs in the DS (globally similar) than the SD (locally similar) condition, and also longer RTs in the SD (locally similar) relative to SS (same object) trials. Fourth, an N2 component between 276 and 330 ms showed differentiation in ERP amplitude among all stimulus conditions. Fifth, source localisation analyses on the ERP data for the N1 time window showed asymmetric bilateral activity with stronger left hemisphere involvement in the DS (globally similar) relative to the SD (locally similar) condition. This left hemisphere activity was largely associated with left posterior temporal-occipital cortex encompassing the medial lingual and posterior fusiform gyri. Analyses of the N2 showed stronger activity in the right occipito-temporal ventral pathway for the SS versus DS (globally similar) condition.

4.1. Early differential sensitivity to local part structure and global shape configuration

These findings support the hypothesis that the perception of complex 3D object shape involves differential processing of local part structure and global shape configuration. This conclusion is supported by three empirical observations from the current study: the differential sensitivity of N1 ERP amplitudes to object similarity defined by local part structure and global shape configuration; the different patterns of behavioural responses to the SD (locally similar) and DS (globally similar) conditions reflected in RTs; and the differences in the distributions of cortical activation revealed by the source localisation analysis. The rationale was that ERP amplitudes can be taken to reflect the degree of perceptual similarity between stimulus pairs in terms of the local part structure and global shape configuration. During the N1 the negative deflections for the SS base objects were more similar to the DS (globally similar) condition than to the SD (locally similar) condition. The behavioural response data also showed that observers took longer to discriminate between SS (base) and DS (globally similar) objects, than between SS (base) and SD (locally similar) objects. This overall pattern extended into the P2. Since the DS (globally similar) condition shares global shape configuration with the SS objects we take these data to reflect (a) early differential sensitivity to global and local shape properties, and (b) more pronounced sensitivity to global shape attributes.

More broadly, the results are consistent with theoretical models that explicitly incorporate distinct levels of representation of higher-order part structure and global spatial configuration (e.g., Behrmann et al., 2006; Behrmann and Kimchi, 2003; Biederman, 1987; Hummel and Stankiewicz, 1996; Marr and Nishihara, 1978). In contrast, the findings challenge models which do not attribute functional significance to these local and global shape properties (e.g., Serre et al., 2007; Ullman, 2006).[2] One interpretation of our results is that processing of local and global shape information during the perception of 3D object shape proceeds in a 'global-to-local' or 'coarse-to-fine' order – consistent with other proposals related to the coarse-to-fine analysis of scene context across spatial scales (e.g., Hegde, 2008; Lamb and Yund, 1993; Peyrin et al., 2003; 2004; 2010; Schyns and Oliva, 1994), and global precedence effects in hierarchical displays (e.g., Navon, 1977). This hypothesis also fits with our observation of late sensitivity to shared local part structure: the SD (locally similar) objects were indistinguishable from the DD objects (in terms of ERP amplitude) during the N1, and were only uniquely identifiable during the N2 between 276–330 ms post-stimulus onset. The 'coarse-to-fine' hypothesis need not imply serial analyses of visual input, but is rather more likely, in the present context, to reflect parallel derivation of local and global shape structure across different time courses (e.g., Bar, 2003; Bar et al., 2006; Bullier, 2001; Heinz et al., 1994, 1998; Peyrin et al., 2003; 2004; 2010). On this account, rapid, coarse, analyses support the derivation of global shape information more quickly than fine-grained local shape information. Image classification decisions may be taken whenever sufficient information has accumulated from either or both processing streams – and in some instances may be based solely on fast, coarse-grained, global shape properties. Such processing may potentially underlie previous observations of ultra-rapid image classification (e.g., Kirchner and Thorpe, 2006; Mouchetant-Rostaing and Giard, 2003; Oram and Perrett, 1992; Thorpe et al., 1996; VanRullen and Thorpe, 2001; Vogels, 1999). Such parallel perceptual analyses of local and global shape attributes provides a further source of recurrent information flow that is consistent with other recent proposals regarding the interaction between feedforward 'bottom-up' analyses of sensory input, and 'top-down' constraints on perceptual processing (e.g., Bar, 2003; Bar et al., 2006; Goddard et al., 2016; Schendan and Ganis, 2015).

In other work, ERP modulations related to local and global processing in hierarchical display (i.e., Navon) tasks have been reported to occur as early as the posterior P1 (Han et al., 2000), but

[2] At the same time, it remains unclear what specific aspects of global shape configuration underlie the early perceptual sensitivity found on the N1 component. This could reflect the 2D global outline derived from bounding contour, the 3D spatial configuration of object parts or (most likely) both (e.g., Arguin and Saumier, 2004; Behrmann et al., 2006; Behrmann and Kimchi, 2003; Lloyd-Jones and Luckhurst, 2002).

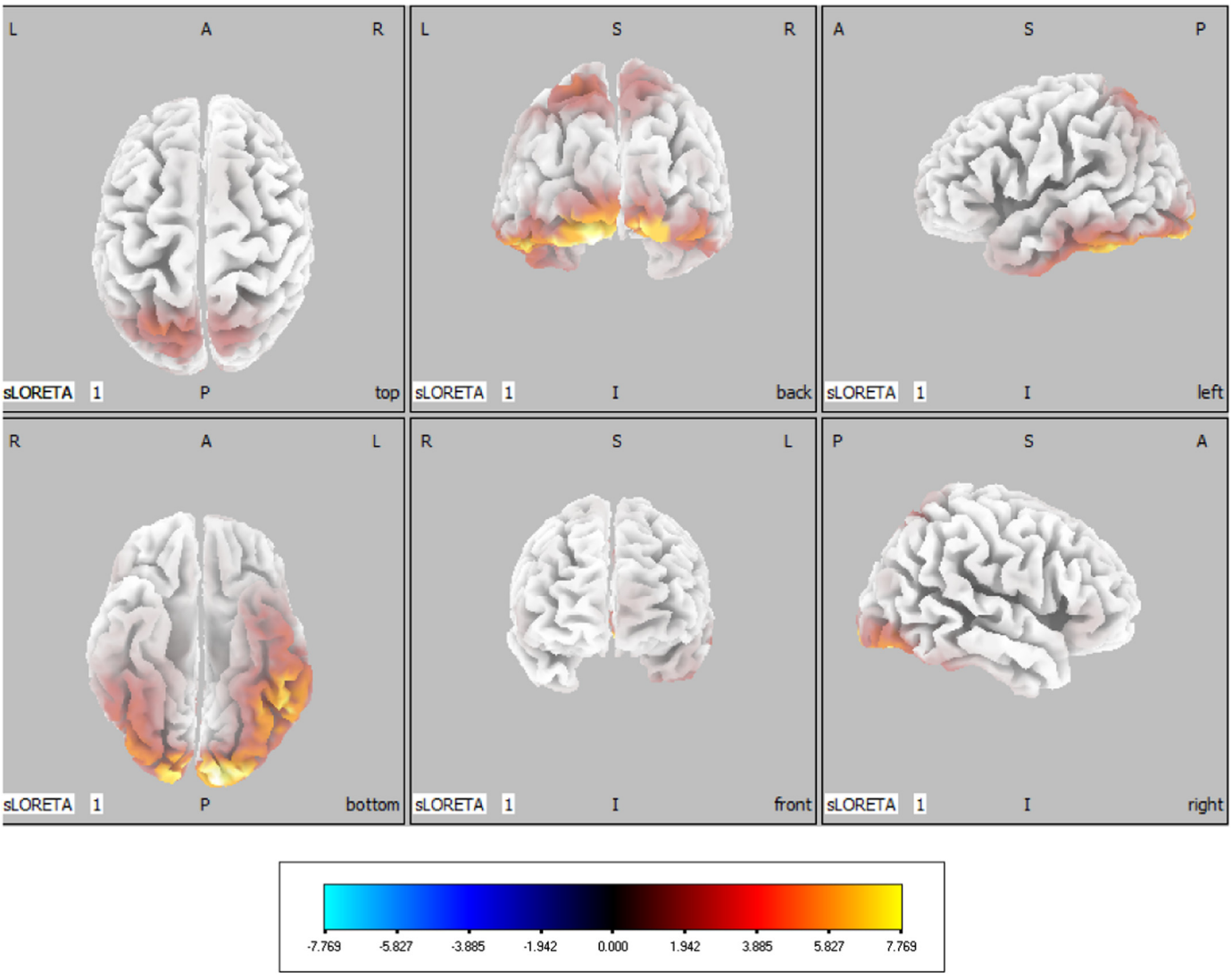

Fig. 7. sLORETA inverse solutions for a pairwise voxel-by-voxel contrast for the SD (locally similar) vs DS (globally similar) conditions during the *N1* (180 ms post-stimulus onset). Significant *t* values (corrected, $p < 0.05$) indicated by the colour coding and plotted in the head model. The axial section shows the left hemisphere on the right (and vice versa). (For interpretation of the references to color in this figure legend, the reader is referred to the web version of this article.)

more frequently around N1/P2 components approximately 150–240 ms post-stimulus onset (e.g., Beaucousin et al., 2013; Proverbio et al., 1998; Yamaguchi et al., 2000). These latter findings are broadly consistent with the present results. However, as noted earlier, it is difficult to determine whether the local/global processes that support performance with hierarchical displays are the same as those involved in the perceptual analysis of 3D object shape at local and global spatial scales. In the standard Navon paradigm, unlike in the present study and in everyday object recognition, observers are explicitly instructed to attend to, and report, incongruent local or global display elements. This incongruence in hierarchical displays is not a typical property of complex 3D objects found in the real world. Even so, our finding of differential N1 sensitivity to the local and global structure of 3D objects converges well with some of this previous work using hierarchical displays, suggesting that these very different tasks (and stimuli) may be tapping into common underlying perceptual mechanisms for the processing of local and global properties of visual sensory input.

4.2. Source localisation

We used source localisation (sLORETA) to provide converging evidence of differential processing. Given the low spatial resolution of sLORETA, caution should be taken when interpreting analyses of the inverse solutions. Even so, the source localisation solutions suggest that the differential sensitivity to local part and global shape configuration found during the N1 originates from partially lateralised neural generators. In particular, we found evidence of asymmetric bilateral activity with stronger left hemisphere involvement in the DS (globally similar) relative to the SD (locally similar) condition. This left hemisphere activity was largely associated with left posterior temporal-occipital cortex encompassing the medial lingual gyrus and posterior fusiform gyrus. Our interpretation of these data is based on a consideration of the types of information that would be most relevant for distinguishing between objects in each condition. Perceptual discrimination between SS and DS (globally similar) objects might be assumed to be more reliant on analyses of local part structure than global shape configuration - since only the former uniquely distinguishes the SS (base) and DS (globally similar) stimuli. In this sense, SS-DS stimulus discrimination can be considered to be 'locally weighted'. In contrast, discrimination between SS and SD (locally similar) objects might be assumed to be more reliant on analyses of global shape configuration – and the SS-SD

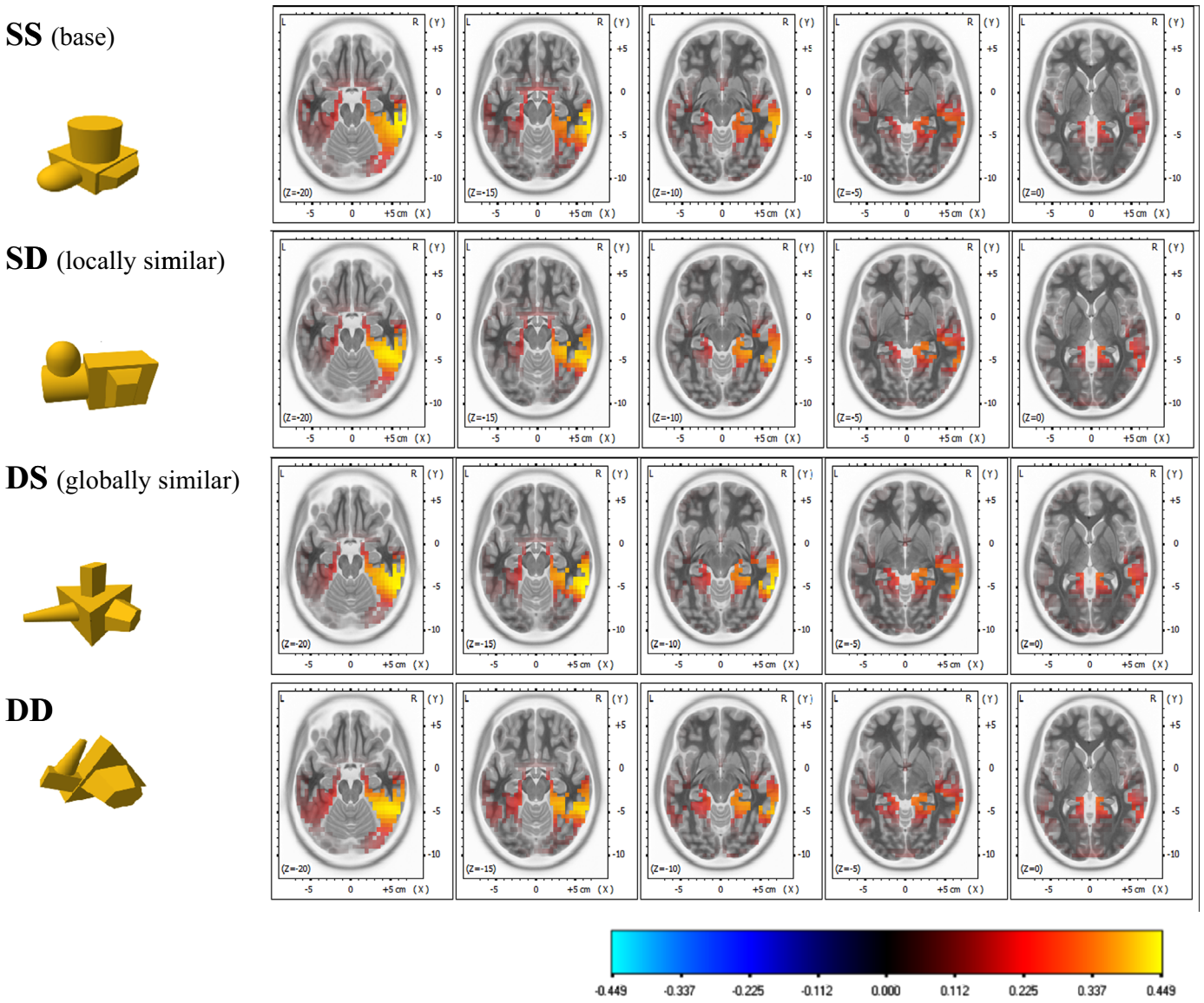

Fig. 8. sLORETA inverse solutions for the *N2* (310 ms post-stimulus onset) component plotted using the MNI1152–2009 T1 template for each stimulus condition. Axial slices (5 mm) shown at Z = −20 to Z = 0. Colour coding shows standardized current density. (For interpretation of the references to color in this figure legend, the reader is referred to the web version of this article.)

discrimination globally weighted. Thus, the stronger left hemisphere activity associated with SS-DS discriminations (relative to SS-SD) may be taken to reflect the weighting of perceptual discrimination in this condition towards local part structure. Interestingly, the SS ('Same' object trials) condition elicited predominantly right hemisphere activity, and was associated with relatively short RTs. This pattern might be assumed to reflect the predominant use of global shape information during 'Same' object trials based on a relatively fast, coarse, analysis of shape information from global processing channels – a hypothesis that is also consistent with slower RTs for rejecting objects in the DS (globally similar) condition.

These findings broadly converge with evidence from functional imaging studies of local and global processing using hierarchical displays (e.g., Fink et al., 1996; 1997), scenes (e.g. Peyrin et al., 2003; 2004; 2010), and work with neuropsychological populations with unilateral brain lesions (e.g., Robertson et al., 1988; Robertson and Lamb, 1991) - which have associated perceptual analyses at local spatial scales more strongly with the left hemisphere. In the current study we found this pattern in a task context involving the perception of complex 3D objects that did not explicitly require observers to attend to, or selectively process, local or global shape information. This supports the hypothesis that the perceptual mechanisms involved in analyses of sensory information across local and global spatial scales may be domain general – that is, not specific to particular stimulus classes.

The left lingual gyrus has been implicated in the processing of face parts (e.g., McCarthy et al., 1999), and shows sensitivity to word length during reading (e.g., Mechelli et al., 2000) – consistent with its involvement in fine scale, parts-based, analyses of sensory input. Of potential relevance also is the proximity of significant voxels in the fusiform gyrus to posterior area V4 (e.g., Bartels and Zeki, 2000 – Table 1; Brincat and Connor, 2004; Pasupathy and Connor, 2001; Roe et al., 2012; Schiller, 1993; Tootell et al., 1998). V4 is a functionally complex area and the subject of considerable current interest. It is thought to play some role in the perception of shape (and other) features during object recognition (e.g., Brincat and Connor, 2004; Pasupathy and Connor, 2001; Roe et al., 2012). Evidence from lesion studies suggests that damage to V4 in monkeys can lead to difficulties in the discrimination of object

a. SS/SD (locally similar)

b. SS/DS (globally similar)

c. SS/DD

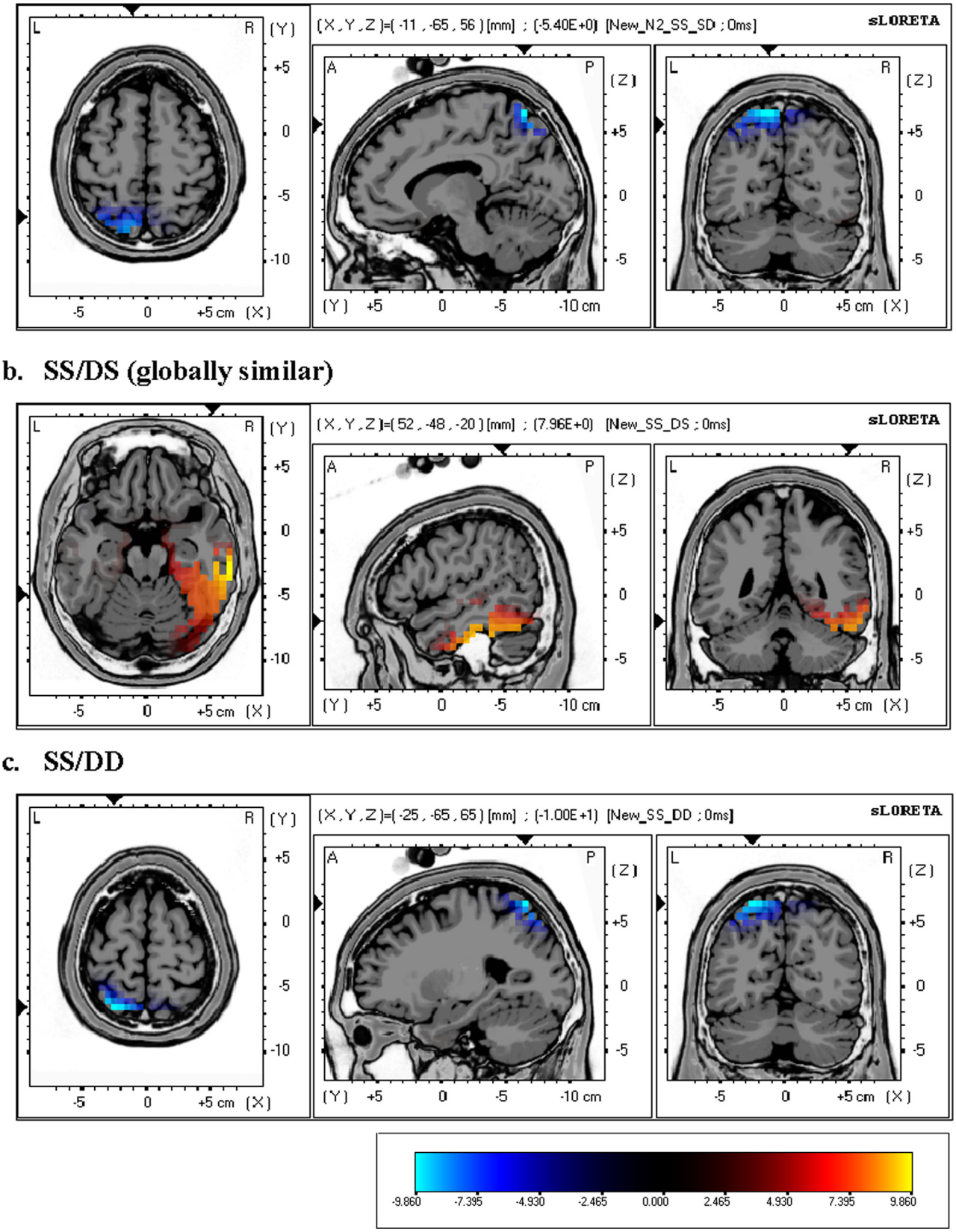

Fig. 9. sLORETA inverse solutions for the difference contrasts between the: (a) SS/SD (locally similar); (b) SS/DS (globally similar) and (c) SS/DD conditions during the N2 (310 ms post-stimulus onset). Co-registered t map plots are colour coded and overlaid onto the 'Colin27' T2 template. The x, y, z coordinate, and *t* value, of the voxels with the largest difference for each contrast are shown. Note that only the SS/DS (globally similar) contrast exceeded the criterion level of significance ($p < 0.05$) after correction. Maps for the SS/SD (locally similar) and SS/DD contrasts are included for completeness. a. SS/SD (locally similar), b. SS/DS (globally similar), c. SS/DD. (For interpretation of the references to color in this figure legend, the reader is referred to the web version of this article.)

shape (e.g., Merigan and Pham, 1998; Schiller, 1993), and in humans to impairments in the integration of stored 'top-down' knowledge and 'bottom-up' perceptual analyses of sensory input during 3D object recognition (e.g., Leek et al., 2012a, 2012b).

4.3. Later components: the N2

Finally, although our primary focus has been on the early differential processing of local and global object shape information reflected in N1/P2 amplitude modulations, the ERPs and inverse solutions for the N2 component merit further discussion. The N2 occurred between 276–330 ms post-stimulus onset and, unlike the N1, showed differentiation in ERP amplitudes between all conditions. One interpretation of this effect in the context of the current task is that it reflects processes related to perceptual discrimination among stimulus pairs. The inverse solutions showed broadly similar bilateral patterns across conditions with greater activity in the right inferior occipito-temporal ventral object pathway. Additionally, further analyses showed stronger activity in the right inferior and middle temporal gyri and fusiform gyrus in the SS than DS (globally similar) condition. We might hypothesise that this pattern of activity reflects processes related to the perceptual matching of global shape attributes.

It is also relevant to consider the similarity of these findings to the Ncl (or 'closure negativity') component reported in other studies (e.g., Doniger et al., 2000', 2001; Sehatpour et al., 2006). The Ncl refers to a bilateral occipito-temporal negativity that commences around 230 ms post-stimulus onset and typically peaks around 290 ms. It is typically observed in tasks of object identification involving the presentation of degraded stimuli, but has also been related to contour integration (Butler et al., 2013). The Ncl correlates with identification accuracy and is thought to reflect the operation of mechanisms associated the recurrent processing of incomplete sensory input during object recognition (Doniger et al., 2000, 2001). The Ncl (and P1, but not the N1) has also been shown to be reduced in schizophrenic patients consistent with a deficit in recurrent processing related to the perceptual integration of local and global image features (e.g., Butler et al., 2013; Doniger et al., 2002). Although the Ncl is typically associated with bilateral occipito-temporal activation and our N2 also comprised stronger right hemisphere activity across all stimulus conditions, one might speculate (Doniger, personal communication) that the differential ERP amplitude modulations found during the N2 relate to recurrent activity supporting the integration of shape information across spatial scales during both object recognition (i.e., matching perceptual input to a long-term memory representation) and, as in the current task, determining the shape equivalence of two perceptual inputs.

5. Conclusions

We investigated the time course of differential perceptual processing of local and global shape information during the perception of 3D objects. Observers made shape matching judgments about pairs of sequentially presented 3D multipart novel objects. ERPs were used to measure online perceptual sensitivity to 3D shape differences in terms of local part structure and global shape configuration. Analyses of the ERP waveforms showed differential sensitivity to shape similarity defined by local part and global shape configuration as early as the N1 component approximately 146–215 ms post-stimulus onset, with differentiation of amplitude modulations among all stimulus types at the N2 component around 276–330 ms post-stimulus onset. Linear inverse solutions computed using sLORETA showed hemispheric asymmetry with stronger involvement of left posterior occipital-temporal cortex in the processing of local part structure. We propose that 3D object shape perception involves parallel processing of information at local and global scales. This processing is characterised by relatively slow derivation of 'fine-grained' local shape structure, and fast derivation of 'coarse-grained' global shape configuration.

Acknowledgements

This investigation was supported by Grants from the Economic and Social Research Council (ESRC: RES-062-23-2075), Experimental Psychology Society (EPS), British Academy and Royal Society to E.C.L., and by a Swiss National Science Foundation Grant (No. 32-1099289) to A.P.

References

Arguin, M., Leek, E.C., 2003. Viewpoint invariance in visual object priming depends on prime-target asynchrony. Percept. Psychophys. 65, 469–477.
Arguin, M., Saumier, D., 2004. Independent processing of parts and of their spatial organisation in complex visual objects. Psychol. Sci. 15, 629–633.
Bar, M., 2003. A cortical mechanism for triggering top-down facilitation in visual object identification. J. Cogn. Neurosci. 15, 600–609.
Bar, M., Kassam, K.S., Ghuman, A.S., Boshyan, J., Schmid, A.M., Dale, A.M., Hamalainen, M.S., Marinkovic, K., Schacter, D.L., Rosen, B.R., Halgren, E., 2006. Top-down facilitation of visual recognition. Proc. Natl. Acad. Sci. USA 103, 449–454.
Bartels, A., Zeki, S., 2000. The architecture of the colour centre in the human visual brain: new results and a review. Eur. J. Neurosci. 12, 172–190.
Beaucousin, V., Simon, G., Cassotti, M., Pineau, A., Houdé, O., Poirel, N., 2013. Global interference during early visual processing: ERP evidence from a rapid global/local selection task. Front. Psychol. 4, 1–6. http://dx.doi.org/10.3389/fpsyg.2013.00539.
Behrmann, M., Kimchi, R., 2003. What does visual agnosia tell us about perceptual organisation and its relationship to object perception? J. Exp. Psychol.: Hum. Percept. Perform. 29, 19–42.
Behrmann, M., Peterson, M.A., Moscovitch, M., Satoru, S., 2006. Independent representation of parts and the relations between them: evidence from integrative agnosia. J. Exp. Psychol.: Hum. Percept. Perform. 32, 1169–1184.
Biederman, I., 1987. Recognition-by-components: a theory of human image understanding. Psychol. Rev. 94, 115–147.
Brincat, S.L., Connor, C.E., 2004. Underlying principles of visual shape selectivity in posterior inferotemporal cortex. Nat. Neurosci. 7, 880–886.
Bullier, J., 2001. Integrated model of visual processing. Brain Res. Rev. 36, 96–107.
Butler, P.D., Abeles, I.Y., Silverstein, S.M., Dias, E.C., Weiskopf, N.G., Calderone, D.J., Sehatpour, P., 2013. An event-related potential examination of contour integration deficits in schizophrenia. Front. Psychol. . http://dx.doi.org/10.3389/fpsyg.2013.00132
Cichy, R.M., Pantazis, D., Oliva, A., 2014. Resolving human object recognition in space and time. Nat. Neurosci. 17, 455–462.
Cristino, F., Davitt, L., Hayward, W.G., Leek, E.C., 2015. Stereo disparity facilitates view generalisation during shape recognition for solid multipart objects. Q. J. Exp. Psychol. 68, 2419–2436.
Davitt, L., Cristino, F., Wong, A., Leek, E.C., 2014. Fixation preference for concave surface discontinuities during object recognition generalises across levels of stimulus classification. J. Exp. Psychol.: Hum. Percept. Perform. 40, 451–456.
Doniger, G.M., Foxe, J.J., Murray, M.M., Higgins, B.A., Javitt, D., 2002. Impaired object recognition and dorsal/ventral stream interaction in schizophrenia. Arch. Gen. Psychiatry 59, 1011–1020.
Doniger, G.M., Foxe, J.J., Schroeder, C.E., Murray, M.M., Higgins, B.A., Javitt, D.C., 2001. Visual perceptual learning in human object recognition areas: a repetition priming study using high-density electrical mapping. NeuroImage 13, 305–313.
Doniger, G.M., Foxe, J.J., Murray, M.M., Higgins, B.A., Snodgrass, J.G., Schroeder, C.E., Javitt, D.C., 2000. Activation time course of ventral visual stream object recognition areas: high density electrical mapping of perceptual closure processes. J. Cognit. Neurosci. 12, 615–621.
Edelman, S., 1999. Representation and Recognition in Vision. MIT Press, Cambridge, MA.
Fabre-Thorpe, M., 2011. The characteristics and limits of rapid visual categorization. Front. Psychol. 2, 1–12.
Fink, G.R., Halligan, P.W., Marshall, J.C., Frith, C.D., Frackowiak, R.S.J., Dolan, R.J., 1996. Where in the brain does visual attention select the forest and the trees? Nature 382, 626–628.
Fink, G.R., Halligan, P.W., Marshall, J.C., Frith, C.D., Frackowiak, R.S.J., Dolan, R.J., 1997. Neural mechanisms involved in the processing of global and local aspects of hierarchical organized visual stimuli. Brain 120, 1779–1791.
Fuchs, M., Kastner, J., Wagner, M., Hawes, S., Ebersole, J.S., 2002. A standardized boundary element method volume conductor model. Clin. Neurophysiol. 113, 702–712.

Goddard, E., Carlson, T.A., Dermody, N., Woolgar, A., 2016. NeuroImage 128, 385–397.
Gratton, G., Cole, M.G.H., Donchin, E., 1983. A new method for off-line removal of ocular artifact. Electroencephalogr. Clin. Neurophysiol. 55, 468–484.
Han, S., He, X., Woods, D.L., 2000. Hierarchical processing and level-repetition effect as indexed by early brain potentials. Psychophysiology 37, 817–830.
Han, S., Weaver, J.A., Murray, S.O., Kang, X., Yund, E.W., Woods, D.L., 2002. Hemispheric asymmetry in global/local processing: effects of stimulus position and spatial frequency. NeuroImage 17, 1290–1299.
Harris, I., Dux, P.E., Benito, C.T., Leek, E.C., 2008. Orientation sensitivity at different stages of object processing: evidence from repetition priming and naming. PLoS One 3 (5), e2256.
Hegde, J., 2008. Time course of visual perception: course-to-fine processing and beyond. Prog. Neurobiol. 84, 405–439.
Heinz, H.J., Johannes, S., Munte, T.F., Magun, G.R., 1994. The order of global- and local-level information processing: electrophysiological evidence for parallel perception processes. In: Heinze, H., Munte, T., Mangun, G.R. (Eds.), Cognitive Electrophysiology. Birkhaeuser, Boston, pp. 1–25.
Heinz, H.J., Hinrichs, M., Scholz, M., Burchert, W., Mangun, G.R., 1998. Neural mechanisms of global and local processing: a combined PET and ERP study. J. Cogn. Neurosci. 10, 485–498. http://dx.doi.org/10.1162/089892998562898.
Holmes, A.P., Blair, R.C., Watson, J.D.G., Ford, I., 1996. Non-parametric analysis of statistical images from functional mapping experiments. J. Cereb. Blood Flow Metab. 16, 7–22.
Hummel, J.E., 2013. Object recognition. In: Reisburg, D. (Ed.), Oxford Handbook of Cognitive Psychology. Oxford University Press, Oxford, pp. 32–46.
Hummel, J.E., Stankiewicz, B.J., 1996. An architecture for rapid, hierarchical structural description. In: Inui, T., McCelland, J. (Eds.), Attention and Performance XVI: On Information Integration in Perception and Communication. MIT Press, Cambridge, MA, pp. 93–121.
Jurcak, V., Tsuzuki, D., Dan, I., 2007. 10/20, 10/10 and 10/5 systems revisited: their validity as relative head-surface-based positioning systems. NeuroImage 34, 1600–1611.
Kimchi, R., Merhav, I., 1991. Hemispheric processing of global form, local form and texture. Acta Psychol. 76, 133–147.
Kirchner, H., Thorpe, SJ., 2006. Ultra-rapid object detection with saccadic eye movements: visual processing speed revisited. Vision Res. 46 (11), 1762–1776.
Lamb, M.R., Yund, E.W., 1993. The role of spatial frequency in the processing of hierarchically organised stimuli. Percept. Psychophys. 54, 773–784.
Leek, E.C., 1998a. The analysis of viewpoint-dependent time costs in visual recognition. Perception 27, 803–816.
Leek, E.C., 1998b. Effects of stimulus viewpoint on the identification of common polyoriented objects. Psychon. Bull. Rev. 5, 650–658.
Leek, E.C., Johnston, S.J., 2006. A polarity effect in misoriented object recognition: the role of polar features in the computation of orientation-invariant shape representations. Vis. Cogn. 13, 573–600.
Leek, E.C., Reppa, I., Arguin, M., 2005. The structure of 3D object shape representations: Evidence from part-whole matching. J. Exp. Psychol.: Hum. Percept. Perform. 31, 668–684.
Leek, E.C., Atherton, C.J., Thierry, G., 2007. Computational mechanisms of object constancy for visual recognition revealed by event-related potentials. Vis. Res. 5, 706–713.
Leek, E.C., Davitt, L., Cristino, F., 2015. Implicit encoding of extrinsic object properties in stored representations mediating recognition: evidence from shadow specific repetition priming. Vis. Res. 108, 49–55.
Leek, E.C., Reppa, I., Rodiguez, E., Arguin, M., 2009. Surface but not volumetric part structure mediates three-dimensional shape representation. Q. J. Exp. Psychol. 62, 814–829.
Leek, E.C., Cristino, F., Conlan, L.I., Patterson, C., Rodriguez, E., Johnston, S.J., 2012b. Eye movement patterns during the recognition of three-dimensional objects: preferential fixation of concave surface curvature minima. J. Vis. 12 (1), 7.
Leek, E.C., d'Avossa, G., Tainturier, M.J., Roberts, D.J., Yuen, S.L., Hu, M., Rafal, R., 2012a. Impaired integration of object knowledge and visual input in a case of ventral simultanagnosia with bilateral damage to area V4. Cogn. Neuropsychol. 29, 569–583.
Lloyd-Jones, T.J., Luckhurst, L., 2002. Outline shape in a mediator of object recognition that is particularly important for living things. Mem. Cogn. 30, 489–498.
Marr, D., Nishihara, H.K., 1978. Representation and recognition of the spatial organization of three-dimensional shapes. Proc. R Soc. Lond. B: Biol. Sci. 200, 269–294.
Mazziotta, J., Toga, A., Evans, A., Fox, P., Lancaster, J., Zilles, K., et al., 2001. A probabilistic atlas and reference system for the human brain: international consortium for brain mapping (ICBM). Philos. Trans. R Soc. Lond. Ser. B: Biol. Sci. 356, 1293–1322.
McCarthy, G., Puce, A., Belger, A., Allison, T., 1999. Electrophysiological studies of human face perception. II: response properties of face-specific potentials generated in occipitotemporal cortex. Cereb. Cortex 9, 431–444.
Mechelli, A., Humphreys, G.W., Mayall, K., Olson, A., Price, C.J., 2000. Differential effects of word length and visual contrast in the fusiform and lingual gyri during reading. Proc. R Soc. Biol. Sci. 267 (1455), 1909–1913.
Merigan, W.H., Pham, H.A., 1998. V4 lesions in macaques affect both single- and multiple-viewpoint shape discriminations. Vis. Neurosci. 15, 359–367.
Mouchetant-Rostaing, Y., Giard, M.H., 2003. Electrophysiological correlates of age and gender perception on human faces. J. Cogn. Neurosci. 15, 900–910.
Navon, D., 1977. Forest before trees: the precedence of global feature in visual perception. Cogn. Psychol. 9, 353–383.
Oram, M.W., Perrett, D.I., 1992. Time course of neural responses discriminating different views of the face and head. J. Neurophysiol. 68, 70–84.
Pascual-Marqui, R.D., 2002. Standardized low resolution brain electromagnetic tomography (sLORETA): technical details. Methods Find. Exp. Clin. Pharmacol. 2002 (24D), 5–12.
Pasupathy, A., Connor, C.E., 2001. Shape representation in area V4 of the macaque: position-specific tuning for boundary confirmation. J. Neurophysiol. 86, 2505–2519.
Peyrin, C., Chauvin, A., Chokron, S., Marendaz, C., 2003. Hemispheric specialization for spatial frequency processing in the analysis of natural scenes. Brain Cogn. 53, 278–282.
Peyrin, C., Baciu, M., Segebarth, C., Marendaz, C., 2004. Cerebral regions and hemispheric specialization for processing spatial frequencies during natural scene recognition: an event-related fMRI study. NeuroImage 23, 698–707.
Peyrin, C., Michel, C.M., Schwartz, S., Thut, G., Seghier, M., Landis, T., Marendaz, C., Vuilleumier, P., 2010. The neural substrates and timing of top-down processes during coarse-to-fine categorization of visual scenes: a combined fMRI and ERP study. J. Cogn. Neurosci. 22, 2768–2780.
Picton, TW., Bentin, S., Berg, P., Donchin, E., Hillyard, SA., Johnson, R., Jr, Miller, GA., Ritter, W., Ruchkin, DS., Rugg, MD., Taylor, MJ., 2000. Guidelines for using human event-related potentials to study cognition: recording standards and publication criteria. Psychophysiology 37 (2), 127–152.
Pizlo, Z., 2008. 3D Shape: Its Unique Place in Visual Perception. MIT Press, Cambridge. MA.
Proverbio, A.M., Minniti, A., Zani, A., 1998. Electrophysiological evidence of a perceptual precedence of global vs. local visual information. Brain Res. 6, 321–334.
Reppa, I., Greville, J., Leek, E.C., 2014. The role of surface-based representations of shape in visual object recognition. Q. J. Exp. Psychol. 68, 2351–2369.
Robertson, L.C., Lamb, M.R., 1991. Neuropsychological contributions to theories of part/whole organisation. Cogn. Psychol. 23, 299–330.
Robertson, L.C., Lamb, M.R., Knight, R.T., 1988. Effects of lesions of temporal-parietal junction on perceptual and attentional processing in humans. J. Neurosci. 8, 3757–3769.
Roe, A.W., Chelazzi, L., Connor, C.E., Conway, B.R., Fujita, I., Gallant, J.L., Lu, Haidong, Vanduffel, W., 2012. Toward a unified theory of visual area V4. Neuron 74, 12–28.
Schendan, H.E., Kutas, M., 2007. Neurophysiological evidence for the time course of activation of global shape, part and local contour representations during visual object categorisation and memory. J. Cogn. Neurosci. 19, 734–749.
Schendan, H.E., Ganis, G., 2015. Top-down modulation of visual processing and knowledge after 250 ms supports object constancy of category decisions. Front. Psychol. . http://dx.doi.org/10.3389/fpsyg.2015.01289
Schiller, P.H., 1993. The effects of V4 and middle temporal (MT) area lesion on visual performance in the rhesus monkey. Vis. Neurosci. 10, 717–746.
Schyns, P.G., Oliva, A., 1994. From blobs to boundary edges: evidence for time and spatial-scale-dependent scene recognition. Am. Psychol. Soc. 5, 195–200.
Sehatpour, P., Molholm, S., Javitt, D.C., Foxe, J.J., 2006. Spatiotemporal dynamics of human object recognition processing: an integrated high-density electrical mapping and functional imaging study of "closure" processes. NeuroImage 29, 605–618.
Sekihara, K., Sahani, M., Nagarajan, S.S., 2005. Localisation bias and spatial resolution of adaptive and non-adaptive spatial filters for MEG source reconstruction. NeuroImage 25, 1056–1067.
Serre, T., Oliva, A., Poggio, T., 2007. A feedforward architecture accounts for rapid categorization. Proc. Natl. Acad. Sci. USA 104, 6424–6429.
Tarr, M.J., Bulthoff, H.H., 1998. Object Recognition in Man, Monkey, and Machine. MIT Press, Cambridge, MA.
Thorpe, S.J., Fize, D., Marlot, C., 1996. Speed of processing in the human visual system. Nature 381, 520–522.
Tootell, RB., Hadjikhani, N., Hall, EK., Marrett, S., Vanduffel, W., Vaughan, JT., Dale, AM., 1998. The retinotopy of visual spatial attention. Neuron. 21 (6), 1409–1422.
Ullman, S., 2006. Object recognition and segmentation by a fragment-based hierarchy. Trends Cogn. Sci. 11, 58–64.
VanRullen, R., Thorpe, SJ., 2001. Time Course of Visual Processing: From Early Perception to Decision-Making. J. Cogn. Neurosci. 13 (4), 445–461.
Vitacco, D., Brandeis, D., Pascual-Marqui, R., Martin, E., 2002. Correspondence of event-related potential tomography and functional magnetic resonance imaging during language processing. Hum. Brain Mapp. 17, 4–12.
Vogels, R., 1999. Categorisation of complex visual images by rhesus monkeys. Part 1: behavioural study. Eur. J. Neurosci. 11, 1223–1238.
Wagner, M., Fuchs, M., Kastner, J., 2004. Evaluation of sLORETA in the presence of noise and multiple sources. Brain Topogr. 16 (4), 277–280.
World Medical Association Declaration of Helsinki, Ethical Principles for Medical Research involving human subjects. Available from: http://www.wma.net/e/policy/b3.htm.
Yamaguchi, S., Yamagata, S., Kobayashi, S., 2000. Cerebral asymmetry of the "top-down" allocation of attention to global and local features. J. Neurosci. 20, RC72.